Supplementary Material: A coupled oscillator model for the origin of bimodality and multimodality

J.D. Johnson[1] and D.M. Abrams[1]
Department of Engineering Sciences and Applied Mathematics, Northwestern University
McCormick School of Engineering and Applied Science
2145 Sheridan Road Evanston, IL 60208

(Dated: 27 June 2019)

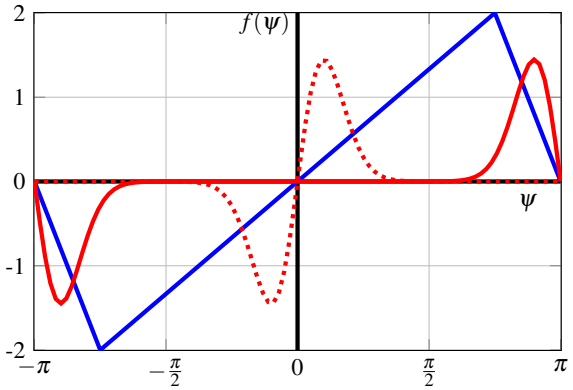

FIG. S1. **Additional interaction functions.** Solid blue curve: triangle wave from Eq. (S1); solid red curve: antisymmetrized variant of the von Mises distribution from Eq. (S2) with $\kappa < 0$; dashed red curve: antisymmetrized variant of the von Mises distribution from Eq. (S2) with $\kappa > 0$. Panels (a) and (b) of Fig. S2 use the triangle wave. Panels (c) and (d) use the antisymmetrized von Mises function, with positive κ (dashed red) in panel (c) and negative κ (solid red) in panel (d). We note that for $\kappa > 0$ the slope at the $\pm\pi$ is never steeper when compared to the origin and for $\kappa < 0$ the slope at the origin is never steeper when compared to the slope at $\pm\pi$.

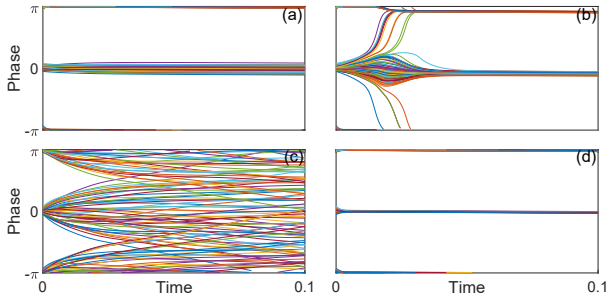

FIG. S2. **Numerical experiments using additional interaction functions.** We test the stability of the bimodal equilibria for alternative coupling functions shown in Fig. S1. (a) Triangle wave coupling with initial fractionation in predicted stable range. (b) Triangle wave coupling with initial fractionation outside predicted stable range. (c) Von Mises coupling with $\kappa > 0$ (expected to be unstable). (d) Von Mises coupling with $\kappa > 0$ (expected to be stable). In all panels $N = 100$ and oscillators' natural frequencies are drawn from the distribution $\mathcal{N}(0,100)$. Initial phases are bimodally distributed with modes at 0 and π, with perturbations ξ_i, $i = 1,\ldots,N$, are drawn from $\mathcal{N}(0,0.01)$.

I. ADDITIONAL COUPLING FUNCTIONS

Figure S1 illustrates two additional coupling functions that we examined. We used a variant of the triangle wave (blue, solid) given by the equation

$$f_{\text{tri}}(u;c) = \begin{cases} \frac{2u}{c} & |u| < c \\ \frac{2u}{c-\pi} - \text{sign}(u)\left(\frac{2\pi}{c-\pi}\right) & c \le |u| \le \pi \end{cases}, \qquad \text{(S1)}$$

assuming that $0 < c < \pi$, and an antisymmetrized variant of the von Mises distribution (red curves) given by

$$f_{\text{vM}}(u;\mu,\kappa) = \sin(u-\mu)\frac{e^{\kappa\cos(u-\mu)}}{2\pi I_0(\kappa)}. \qquad \text{(S2)}$$

We numerically probe the stability of the bimodal equilibrium using these interaction functions in Fig. S2. Here $N = 100$, the oscillators' frequencies are drawn from a distribution $\mathcal{N}(0,100)$, the phase perturbation, ξ_i, is drawn from the distribution $\mathcal{N}(0,0.01)$ and we set $K = -1000$. In panels (a) and (b) we take the triangle wave defined in Eq. (S1) and set $c = 3\pi/4$; this gives a stable fractionation threshold $1/4 < x < 3/4$. We test that threshold numerically by setting $x_{\text{initial}} = 7/10 < 3/4$ in panel (a) and $x_{\text{initial}} = 8/10 > 3/4$ in panel (b). As expected, we see that the fractionation is stable in panel (a) and is unstable in panel (b).

In panels (c) and (d) we use the antisymmetrized von-Mises function from Eq. (S2) with $\mu = 0$ and $x_{\text{initial}} = 1/2$. In panel (c) we set $\kappa = 10$, and, as expected, we see that the bimodal equilibrium appears unstable; this is because there does not exist a range of x such that Eq. (10) can be satisfied given that the slope at the origin is far steeper than the slope at the $\pm\pi$. We note that in (c) the system appears to tend to the incoherent state. In panel (d) we set $\kappa = -10$ and observe that the bimodal state appears to be stable under perturbation, which is expected given that the slope at the $\pm\pi$ is steeper when compared to the origin.

II. BASINS OF ATTRACTION FOR MULTIMODAL STATES

We have conducted some preliminary numerical exploration of the sizes of basins of attraction for various equilibria for the example interaction function given in Eq. (11) of the main text. We simulated the system one hundred times with initial phases chosen independently at random from the

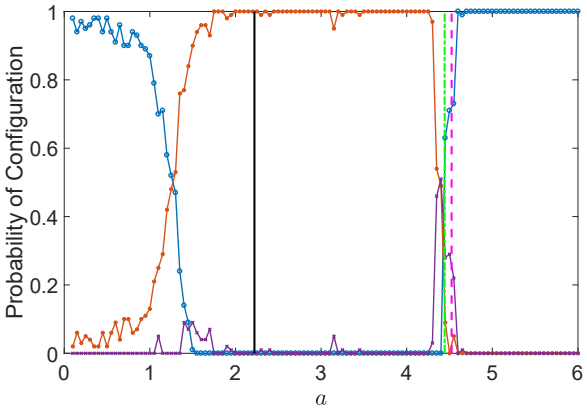

FIG. S3. **Basins of attraction**. We plot the fraction of uniform random initial conditions that end up in bimodal (blue circles), trimodal (orange asterisks), or higher order multimodal (purple xs) states for the concrete system examined in the main text. Here $N = 100$, $K = -10000$ and oscillators' natural frequencies are drawn from the distribution $\mathcal{N}(0,100)$. We performed 100 unique simulations for each value of a. Final states (presumed equilibria) were identified automatically via k-means clustering. Thresholds given in the main text for stability of bimodality and the antiphase state are given by the solid black line and the dot-dashed green line, respectively. The threshold for the necessary condition for stability of the trimodal state is given by the vertical dashed magenta line.

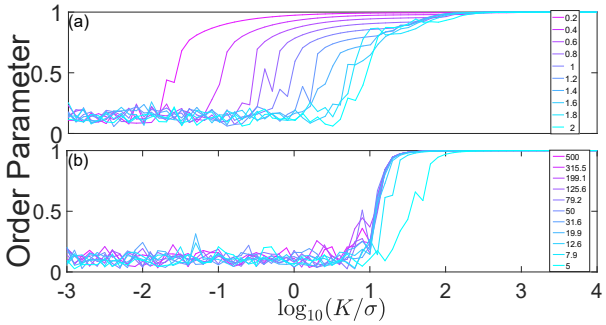

FIG. S4. **Critical coupling strength**. We perform numerical experiments to demonstrate the existence of a critical coupling strength for our system and evaluate its dependence on parameter a using the interaction function defined in Eq. (11) of the main text. Here $N = 100$, the natural frequency distribution is given by $\mathcal{N}(0,\sigma^2)$, and the initial phase distribution is $\rho(\theta) = 0.5\delta(\theta) + 0.5\delta(\theta - \psi_0)$, where ψ_0 is the predicted phase separation given by the stable fixed points of Eq. (11). Here, each curve represents a different value of a (values indicated in legend). As in the standard Kuramoto model, the critical coupling strength is dependant on the size of the standard deviation of the distribution, but unlike the standard Kuramoto model, it appears to also depend on a, which sets the shape of the interaction function.

uniform distribution over the circle, i.e. $\mathcal{U}(-\pi,\pi]$, and evaluated the fraction of the time that the system converged to each distinct equilibrium state. Results are shown in Fig. S3, with $N = 100$, $K = -10000$, and oscillator natural frequencies drawn from the distribution $\mathcal{N}(0,100)$.

Fig. S3 also shows the stability thresholds described in Eqns. (12) (bimodal state), (A.13) (antiphase state), and trimodal state (A.12) of the main text, visualized by the solid black, and dot-dashed green, and magenta vertical lines respectively. In order to classify the observed equilibria, we use a k-means algorithm on the unit circle, with the number of clusters, k, being decided by the gap statistic. We say that a equilibrium state is bimodal if $k = 2$, trimodal if $k = 3$, and so on.

We note that the results are consistent with our analysis in that the probability of a configuration is always zero in ranges of a where it is excluded. Although, we have not analyzed equilibria with more than three modes, we observe that such modes are unlikely to be observed for most values of a, and thus have apparently small basins of attraction.

Given that this experiment was conducted with heterogeneous oscillators, this lends plausibility to the idea that the system will end up in a multimodal state for sufficiently large coupling. More formal analysis of the basin size of the bimodal and trimodal state will be left for future work.

III. CRITICAL COUPLING STRENGTH

In the standard Kuramoto model with attractive coupling, there exists a critical coupling strength K_c at which the system bifurcates from an incoherent state to the ordered state. To look for K dependence in the system detailed in main text, we examine the simplest cases of $N = 2$ and $N = 3$, and also conduct several numerical experiments with results shown in Fig. S4, though we leave more thorough exploration for future work.

Figure S4 shows how order varies as we increase coupling strength among nonidentical oscillators with the concrete interaction function used in the main text. Here, we set $N = 100$ and draw the frequencies from the distribution $\mathcal{N}(0,\sigma^2)$. From here, we vary the quantity K/σ so that $\log_{10}(K/\sigma)$ runs from -2 to 4. Each curves shown above represents the result of an experiment for a given value of a. Here, the order parameter is defined as follows:

$$R = \max\left\{\left|\sum_j \frac{e^{2i\theta_j}}{N}\right|, \left|\sum_j \frac{e^{3i\theta_j}}{N}\right|, \left|\sum_j \frac{e^{\frac{2\pi}{a}i\theta_j}}{N}\right|\right\}. \tag{S3}$$

Defining the order parameter in this fashion sets the value of the order parameter to be 1 whenever the final configuration is bimodal or an equally spaced trimodal solution. Just as in the standard Kuramoto model, if the coupling strength K is not sufficiently large in magnitude, the system goes to the incoherent state due to intrinsic oscillator heterogeneity. We observe that the critical coupling strength appears to be proportional to the standard deviation of the frequency distribution, similar to the result in the standard Kuramoto analysis, but we point out that the critical coupling strength K_c also appears to have

dependence on the value of a. We believe that some insight into this dependence can be gained from examining the simple $N = 2$ and $N = 3$ cases, though more rigorous analysis is left for future work.

For $N = 2$, the system reduces to

$$\dot{\psi} = \Delta\omega - Kf(\psi) \tag{S4}$$

where $\Delta\omega = \omega_2 - \omega_1$. Setting $\dot{\psi} = 0$, we find that a fixed point ψ_0 must satisfy the equation:

$$\frac{\Delta\omega}{K} = f(\psi_0)\,. \tag{S5}$$

Note, this fixed point does not always exist, but if the coupling function f has zeros, a fixed point must arise as $|K| \to \infty$.

Even without explicitly defining ψ_0, we can observe scaling dependencies for the critical coupling strength K_c, which is defined such that

$$f(\psi_{max}) = \frac{\Delta\omega}{K_c} \tag{S6}$$

where $\psi_{max} \in (-\pi, \pi]$ is the value such that $f(\psi_{max}) = \max f(\psi)$ (the arg max). We observe that $K_c \propto \Delta\omega$, which is expected if $K_c \propto \sigma$ as in the standard Kuramoto model (since for two oscillators $\sigma \propto \Delta\omega$) and is observed in our numerical experiments even for $N \gg 2$.

We also observe that K_c scales with the maximum value of the interaction function f, which in our numerical experiments depends on the parameter a. Similar dependence is also evident if we consider the $N = 3$ case.

For $N = 3$, we take the natural frequencies (without loss of generality) to be $0, -\sigma/3, \sigma/3$ respectively. As before, we convert to difference coordinates $\psi_1 = \theta_2 - \theta_1$ and $\psi_2 = \theta_3 - \theta_2$, and arrive at two conditions for existence of equilibria:

$$\frac{\sigma}{K} = f(\psi_2 - \psi_1) - f(\psi_2) - 2f(\psi_1) \tag{S7}$$

$$\frac{\sigma}{K} = f(\psi_2 - \psi_1) + 2f(\psi_2) + f(\psi_1)\,, \tag{S8}$$

which simplify to

$$\frac{\sigma}{K} = f(\psi_2 - \psi_1) + f(\psi_2) \tag{S9}$$

$$f(\psi_1) = -f(\psi_2)\,. \tag{S10}$$

Hence, a necessary condition K must satisfy for the existence of equilibria is

$$\frac{\sigma}{K} \leq 2f(\psi_{max})\,. \tag{S11}$$

So, just as in the $N = 2$ case, we see that the critical coupling strength K_c is proportional to the oscillator heterogeneity σ and inversely proportional to the maximum of the interaction function f.

We hypothesize that similar scaling laws hold for $N \gg 1$, and find that such a hypothesis is consistent with data from numerical experiments shown in Fig. S4.